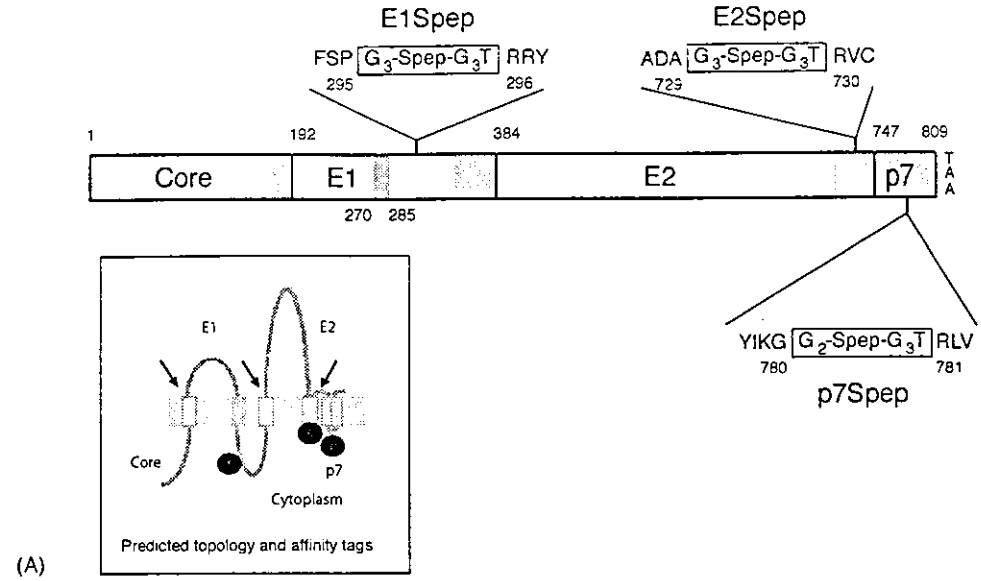

Detail of E1 glycoprotein

```
        200                 220                 240                 260        270                 285                 300
YEVRNVSGIYHVTNDCSNSSIVYEAADVIMHAPGCAPCVRENNSSRCWVALTPTLAARNASVPTTTLRRHVDLLVGTAAFCSAMYVGDLCGSVFLISQLFTFSPRRHET
                                                                                MMMMMMMMMMMMMMMMM

                    320                 340                 360                 380
VQDCNCSIYPGHVSGHRMAWDMMMNWSPTAALVVSQLLRIPQAVMDMVAGAHWGVLAGLAYYSMVGNWAKVLIVMLLFAGVDG
                                    MMMMMMMMMMMMMMMMMMMMMMMMMMMMMMMM
```

(B)

Fig. 1. The HCV structural polyprotein. (A) Schematic representation of the N-terminus encoding the Core, E1, E2 and p7 proteins; translation is terminated by an engineered termination codon (TAA) after p7. Amino acid numbering is shown, and transmembrane helical regions are indicated by shading. The putative internal transmembrane domain in E1 (aa 270–284) is darkened. The positions of the respective Spep tags are shown. The insert (lower left) contains a schematic showing the predicted membrane topology of the Core-E1-E2-p7 polyprotein including the polytopic form of the E1 glycoprotein. The respective Spep tags are shown as black balls. Arrows denote signal peptide cleavage sites in the polyprotein. (B) Amino acid sequence of the E1 glycoprotein. Transmembrane regions predicted by the PHD-htm algorithm (Rost et al., 1995); accessed at (Columbia University Bioinformatics Center, 2002) are indicated by *M*'s under the amino acid sequence. Only extended regions identified with ≥90% probability are shown. Potential glycosylation sites are underlined.

provided by Z.-Y. Keck and S.K.H. Foung (Stanford University). Of these, only H-111 is able to recognize its respective protein in Western blot analysis (Z.-Y. Keck and S.K.H. Foung, unpublished). The other human MAbs recognize conformational determinants (Hadlock et al., 2000). Control studies utilized human MAbs directed against HIV-1 gp120 (447-52D, from S. Zolla-Pazner (Conley et al., 1994)) and gp41 (F240, from M. Posner (Cavacini et al., 1998)) and a murine anti-gp41 MAb (Chessie 8, from G. Lewis (Abacioglu et al., 1994)).

2.3. Characterization of affinity-tagged HCV glycoproteins

HCV expression plasmids were used to transiently transfect monkey COS cell using FuGENE-6 (Roche Biochemicals) reagent (Lu et al., 2001). In some experiments, cells were metabolically labeled for the final 16 h in 5 ml of cysteine- and methionine-free Dulbecco's Modified Eagle Medium containing 2% dialyzed fetal bovine serum and 125 μCi each ^{35}S-methionine and ^{35}S-cysteine (Amersham Life Sciences). Cells were harvested 48 h after transfection and lysed in solubilization buffer comprising 20 mM Tris–HCl, 100 mM ammonium sulfate, 10% glycerol (Mirzabekov et al., 2000), 0.5% cyclohexyl-pentyl-β-D-maltoside (Cymal-5; Anatrace, Maumee, OH) nonionic detergent and protease inhibitors (Complete Protease Inhibitor Tablets; Roche Diagnostics). Preliminary studies explored the use of other nonionic and zwitterionic detergents (Cymal-5, Triton X-100, Brij-97, and CHAPSO; 0.5% and 1%) and 0.5% Cymal-5 was chosen based on its efficiency in extracting noncovalently associated E1–E2 heterodimers and its high critical micellar concentration (to facilitate dialysis in the subsequent formation of proteoliposomes). In many studies, the solubilization buffer also contained 1 mM DTT (Tatu et al., 1993).

Spep-tagged proteins were isolated using S-protein agarose (SAG) beads (Novagen, Inc., Madison, WI). Briefly, cleared cell lysates (300–500 μl) were incubated with SAG beads (100 μl of slurry) at 4 °C for at least 1 h and the beads were subsequently washed in solubilization buffer. The affinity-purified material was typically eluted by boiling in Laemmli SDS-PAGE sample buffer, in the pres-

ence or absence of 100 mM DTT. Deglycosylation of the affinity-purified material using PNGase F (New England Biolabs, Beverly, MA) was performed as recommended by the manufacturer. Immunoprecipitation of Spep-tagged and untagged HCV envelope glycoproteins from cell lysates (500 μl) utilized 5 μg of the human MAbs. Immune complexes were precipitated using protein A–Sepharose (100 μl of a 50% v/v slurry; Sigma).

Proteins were resolved by SDS-PAGE and detected by phosphorimaging or by Western blot analysis using either S-protein horseradish peroxidase (S-HRP; Novagen, Inc.) or murine MAbs with an HRP-conjugated second antibody. Western blots were visualized by chemifluorescence using ECL-Plus (Amersham Biosciences) and quantitated by fluorescence imaging. Quantitative analyses were performed using the Fuji FLA3000G imager and Image Gauge software (Fuji).

2.4. S-protein paramagnetic beads and proteoliposomes

M-270 carboxylic acid Dynabeads (Dynal AS, Lake Success, NY) were activated using carbodiimide chemistry and coupled to S-protein (RNS2; Biozyme Laboratories, San Diego, CA) using methods recommended by Dynal AS. Spep-tagged HCV glycoproteins were isolated from cell lysates by overnight incubation with beads at 4 °C. Typically, 5×10^7 beads were used per 500 μl of cell lysate in order to obtain a dense coverage. The paramagnetic beads were subsequently washed extensively and maintained for up to 1 month in solubilization buffer at 4 °C. The nonionic detergent was included in all subsequent immunochemical analyses of the beads.

Lipids were obtained as chloroform solutions from Avanti Polar Lipids (Alabaster, AL). A total of 10 mg of lipids {1-palmitoyl-2-oleoyl-*sn*-glycero-3-phosphocholine (POPC), 1-palmitoyl-2-oleoyl-*sn*-glycero-3-phosphoethanolamine (POPE), and dimyristoylphosphatidic acid (DMPA), mixed in a molar ratio of 6:3:1} were dried in a glass vial under a vacuum until all of the solvent was removed. One milliliter of phosphate-buffered saline (PBS) was added to the tube, and a liposomal suspension was obtained by 1–2-min ultrasonication in an ice bath. A stock of the fluorescent lipid dioleoylphosphoethanolamine–lissamine rhodamine B (Rhodamine–DOPE) was similarly prepared, at a final concentration of 1 mg ml^{-1}, and used as a tracer to assess lipid accretion. All liposomal stocks were kept in liquid N_2 until use.

Proteoliposomes were produced using methods described by Sodroski and colleagues (Mirzabekov et al., 2000) and modified in our laboratory. In brief, the liposomal solution was added to a suspension of paramagnetic beads bearing the affinity-purified HCV envelope glycoproteins, and the Cymal-5 nonionic detergent was slowly removed by dialysis to enable proteoliposome formation. Considerable evidence supports the model that during solubilization, the nonionic detergent binds to transmembrane domains and replaces the membrane; in reconstitution, this process is reversed (see review (Rigaud et al., 1995)). Fifty million paramagnetic beads and 50 μl of the 10 mg ml^{-1} liposome stock were mixed in 0.5 ml of solubilization buffer for 1 h at 4 °C before dialysis was initiated. Dialysis using a 10 kDa molecular weight cutoff cassette (Slide-A-Lyzer 10 K, Pierce, Rockford. IL) was carried out for 24 h at 4 °C against two changes of solubilization buffer lacking both detergent and protease inhibitors. Beads were then isolated magnetically and washed before storage in PBS containing 0.1% bovine serum albumin (BSA). Proteoliposome were stable for over 3 months at 4 °C, and were routinely washed into PBS (lacking BSA) prior to use.

Preliminary optimization and quality control studies for proteoliposome formation utilized the lipid mixture containing a tracer of Rhodamine–DOPE (1% w/w). Lipid was subsequently solubilized from the proteoliposomes and the amount of Rhodamine–DOPE tracer was determined spectrophotometrically. Approximately 60 μg of lipid could be deposited on 10^8 beads containing Spep-tagged transmembrane protein, sufficient to saturate the surface area of the beads (estimated at 50 μg (Mirzabekov et al., 2000)). Preliminary studies demonstrated that lipid accretion onto paramagnetic S-protein beads required that a transmembrane protein be bound (CTM and JHN; unpublished). Reports from numerous laboratories have demonstrated the robust utility of this methodology in reconstituting functional and antigenically intact transmembrane glycoproteins (see Babcock et al., 2001; Grundner et al., 2002; Mirzabekov et al., 2000; Rigaud et al., 1995; Walter et al., 1990).

2.5. Flow cytometric analysis of paramagnetic beads

Flow cytometry was performed using a FACSCalibur instrument (BD Biosciences). Paramagnetic beads ($\approx 5 \times 10^5$) containing affinity-purified HCV envelope glycoproteins in solubilization buffer (with 0.5% Cymal-5) or proteoliposomal beads ($\approx 5 \times 10^5$) in PBS and 0.1% BSA were incubated with 5 μg of the primary murine or human MAb in 50 μl for 1 h on ice and then washed in their respective buffers prior to incubation with the appropriate secondary antibody (CalTag, Burlingame, CA) at room temperature for 30 min. The murine MAbs were detected using a phycoerythrin-conjugated goat antibody, and the human MAbs were detected using a fluorescein-conjugated goat antibody. Both protein and proteoliposomal beads were ultimately washed into 1 ml of PBS for flow cytometric analysis.

3. Results

3.1. Selection of sites for affinity tags in the HCV envelope glycoproteins

In these studies, we sought to identify sites within E1, E2 and p7 that could accommodate the insertion of an affinity

tag without disrupting the biochemical and immunochemical properties of the noncovalently associated E1–E2 complex. We examined three sites with the potential for exposure on the cytosolic face of the membrane.

In the case of the polytopic p7 protein, which contains two hydrophobic membrane-spanning domains separated by a short cytoplasmic region (Carrere-Kremer et al., 2002), the affinity tag was introduced between charged amino acids in the cytoplasmic loop (Fig. 1A). Although the C-terminal regions of the E1 and E2 glycoproteins also contain charged amino acids embedded within hydrophobic transmembrane domains (Cocquerel et al., 2000), these residues are believed to lie within the membrane. It has been proposed that these charged residues play a role in reorienting the C-termini from the lumenal to cytosolic side of the ER following signal peptidase cleavage (Cocquerel et al., 2002; Op De Beeck et al., 2001). To explore this latter model in the E2 glycoprotein, we introduced the affinity tag between charged residues in the transmembrane domain of E2 (Fig. 1A), anticipating that this would severely disrupt biogenesis.

The E1 glycoprotein presented an unusual opportunity to probe structural and topologic aspects of biogenesis. Using predictive computer algorithms trained to identify transmembrane helices (Rost et al., 1995), we found evidence for a potential transmembrane helix internal to the E1 glycoprotein, between amino acid residues 270–284 (Fig. 1B). This raised the possibility that the E1 glycoprotein might contain two membrane-spanning regions — the well-documented C-terminal domain and the predicted internal domain — separated by an intervening cytoplasmic loop. This suggestion was consistent with earlier studies in which an internal hydrophobic region was shown to be involved in membrane association (Matsuura et al., 1994). Cytosolic exposure of the E1 glycoprotein has been suggested as the basis for interaction with the virion Core protein (Lo et al., 1996; Merola et al., 2001). Based on these theoretical and experimental suggestions, we introduced the affinity tag in the predicted cytoplasmic loop, between amino acids 295 and 296 (Fig. 1A).

3.2. Expression of the HCV envelope glycoproteins

The infectious HCV cDNA (genotype 1b) was originally isolated from an infected individual (Aizaki et al., 1998) and the region encoding the N-terminal polyprotein (Core, the E1 and E2 glycoproteins and p7) was used in these studies. The 15 amino acid S-peptide affinity tag (Spep) is derived from the small subtilisin-generated fragment of ribonuclease A and binds with high affinity to its ligand, the larger ribonuclease fragment (S-protein) (Kim and Raines, 1993; Richards and Vithayathil, 1959). This peptide was chosen based on its ability to function as an affinity tag when inserted internally within the protein of interest (JHN, unpublished). When transfected into simian COS-7 cells, the three tagged constructs (E1Spep, E2Spep and p7Spep; Fig. 1A) were expressed at levels comparable to the untagged

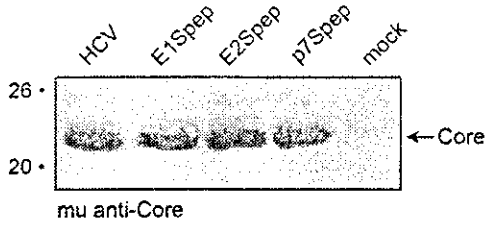

Fig. 2. Expression of HCV Core from Spep-tagged and untagged polyprotein. COS cells expressing the E1Spep, E2Spep or p7Spep polyproteins, or the untagged HCV polyprotein were lysed in solubilization buffer, and proteins were resolved by SDS-PAGE. The Western blot was probed using a pool of murine anti-Core MAbs (#c11-7, #c11-10 and #c11-14; indicated below the image as mu anti-Core). Molecular weight markers are shown at left.

HCV construct and all polyprotein expression resulted in the accumulation of proteolytically processed mature Core protein (Fig. 2).

We then examined the biosynthesis of the envelope glycoproteins to determine the effects of the affinity tag on protein processing, folding and assembly. Cells were lysed using 0.5% Cymal-5 nonionic detergent and the tagged glycoproteins were isolated using S-protein agarose (SAG) beads. In all cases, both E1 and E2 glycoproteins could be co-isolated, regardless of the position of the affinity tag (Fig. 3A). By far the highest recovery of E1–E2 complex was from the E1Spep polyprotein, and lower amounts were isolated from the p7Spep and E2Spep polyproteins, respectively. The expressed glycoproteins were further characterized by using peptide N-glycosidase F (PNGase F) to generate the fully deglycosylated proteins. In all cases, the E1 polypeptide was detected as a single band of the appropriate molecular weight (data not presented). The pattern of E2 polypeptides was, however, more complex (Fig. 3B). In the case of the E1Spep polyprotein, a discrete 40 kDa band corresponding to authentic E2 polypeptide was observed, as well as a series of more slowly migrating species. By contrast, the discrete band was absent in the E2Spep and p7Spep polyprotein products and only the more slowly migrating species were seen. Based on previous reports (Lin et al., 1994; Mizushima et al., 1994), we suspected that one or more of the slowly migrating species might represent unprocessed E2–p7 precursor. To further examine this question, we modified the E1Spep construct by introducing a stop codon at the E2–p7 junction to ablate expression of p7. The slowly migrating species vanished and only the authentic E2 polypeptide remained (Fig. 3C). These results confirm that the more slowly migrating species represent forms of the uncleaved E2–p7 precursor. Therefore, we concluded that the E2Spep and p7Spep polyproteins were largely defective in signal peptidase cleavage at the E2–p7 junction. By contrast, the E1Spep polyprotein was able to undergo proteolytic processing to yield mature E1 and E2 glycoproteins.

To assess the state of protein folding in the E1Spep-E2 complex, we examined the mobility of the E2 glycoprotein by SDS-polyacrylamide gel electrophoresis (SDS-PAGE)

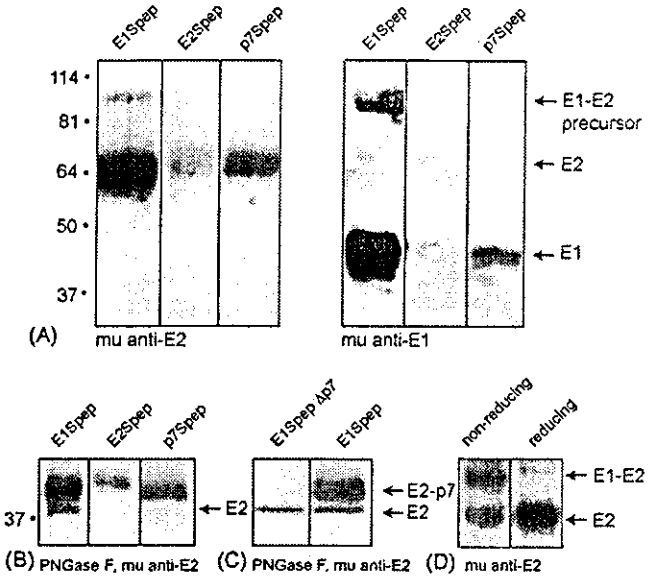

Fig. 3. Characterization of Spep-tagged HCV envelope glycoproteins. Expressed proteins were precipitated using S-protein agarose (SAG) and Western blots were visualized using murine MAbs directed to either E1 (MAbs #299 and #384) or E2 (MAbs #187) as indicated below the image (mu anti-E1 or mu anti-E2, respectively). Molecular weight markers are indicted at left. (A) Isolation by SAG precipitation of E2 (left) and E1 (right) from cells expressing E1Spep, E2Spep and p7Spep. The mature E1 and E2 glycoproteins are indicated at right; residual unprocessed E1–E2 precursor is also visible. (B) Isolated glycoproteins were deglycosylated using PNGase F and E2-reactive polypeptides were detected using murine anti-E2 MAb. The expected position of the E2 polypeptide is indicated. (C) p7 Expression was ablated from the E1Spep polyprotein by introducing a stop codon at the E2–p7 junction (E1SpepΔp7). Glycoproteins were deglycosylated using PNGase F and E2 polypeptides were detected using murine anti-E2 MAb. E2 and E2–p7 polypeptides are indicated. (D) The E1–E2 complex from E1Spep polyprotein was isolated and resolved by SDS-PAGE under non-reducing or reducing conditions. The E2 glycoprotein and the disulfide-crosslinked E1–E2 complex are indicated.

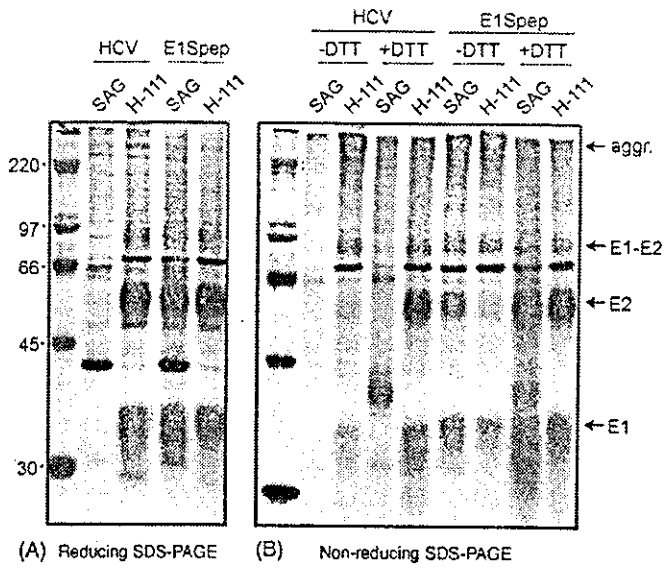

Fig. 4. Isolation of noncovalently associated E1–E2 complex under mildly reducing conditions. Cells expressing the untagged HCV structural polyprotein or the E1Spep polyprotein were metabolically labeled using ^{35}S-methionine and -cysteine and lysed in solubilization buffer with (+DTT) or without (−DTT) 1 mM DTT. E1–E2 complexes were precipitated using either SAG or a human anti-E1 MAb H-111. Isolated proteins were resolved by SDS-PAGE under reducing (A) or non-reducing (B) conditions. Free E1 and E2 are indicated, as are the covalently linked E1–E2 complex/precursor (E1–E2) and the higher molecular weight aggregates (aggr.). Cells expressing the untagged HCV polyprotein served as control for the SAG precipitation. ^{14}C-labeled molecular weight markers (Amersham Biosciences) are shown at left. The identity of the additional bands (≈ 40 and 70 kDa) is unknown.

under nonreducing conditions. In these experiments, the misfolded disulfide-crosslinked E1–E2 complex migrates slowly, whereas the noncovalently associated E2 migrates as the free glycoprotein. From these studies (Fig. 3D), we estimated that ≈25% of the E2 glycoprotein isolated by using the E1Spep tag was in the form of noncovalently associated complex. Although this percentage is similar to that reported for the untagged HCV polyproteins (Deleersnyder et al., 1997; Dubuisson et al., 1994; Dubuisson and Rice, 1996 and see below), we were surprised at the extent of apparent misfolding.

In order to investigate the source of the disulfide-crosslinked aggregates commonly found upon expression of the HCV envelope glycoproteins, we modified our cell lysis buffer to include 1 mM DTT. We reasoned that this low level of reducing agent might mitigate against the oxidative environment in the ER (Tatu et al., 1993) but would itself be unable to reduce properly folded protein. If proper folding of the expressed glycoproteins were limited kinetically, then this low level of reducing agent might enhance the isolation of properly folded, noncovalently associated complex. We explored this hypothesis using both the native, untagged HCV structural polyprotein and the affinity-tagged E1Spep polyprotein. Cells were metabolically labeled and lysed in the presence or absence of 1 mM DTT. Complexes were then immunoprecipitated using either SAG, or a human anti-E1 MAb H-111 (Z.-Y. Keck and S.K.H. Foung; unpublished). Overall yields were similar in the presence or absence of DTT and lysis in the presence of 1 mM DTT did not disrupt the E1–E2 association (Fig. 4A). As analyzed by SDS-PAGE under reducing conditions, comparable amounts of E1–E2 complex were isolated by H-111 from cells expressing the tagged or untagged HCV polyprotein, suggesting retention of the MAb epitope. Importantly, both tagged and untagged complexes isolated in the presence of 1 mM DTT were largely noncovalently associated (Fig. 4B). By contrast, samples prepared in the absence of 1 mM DTT showed significant amounts of E1–E2 aggregation, and commensurately lesser amounts of noncovalently associated E1 and E2.

We speculate that lysis under mildly reducing conditions may prevent artefactual disulfide bond formation during isolation or, more likely, may facilitate disulfide bond reshuffling in the nascent complex. We presume that, in the absence of competing and irreversible disulfide bond formation, the glycoprotein complex in the presence of 1 mM DTT is able to fold into its native state.

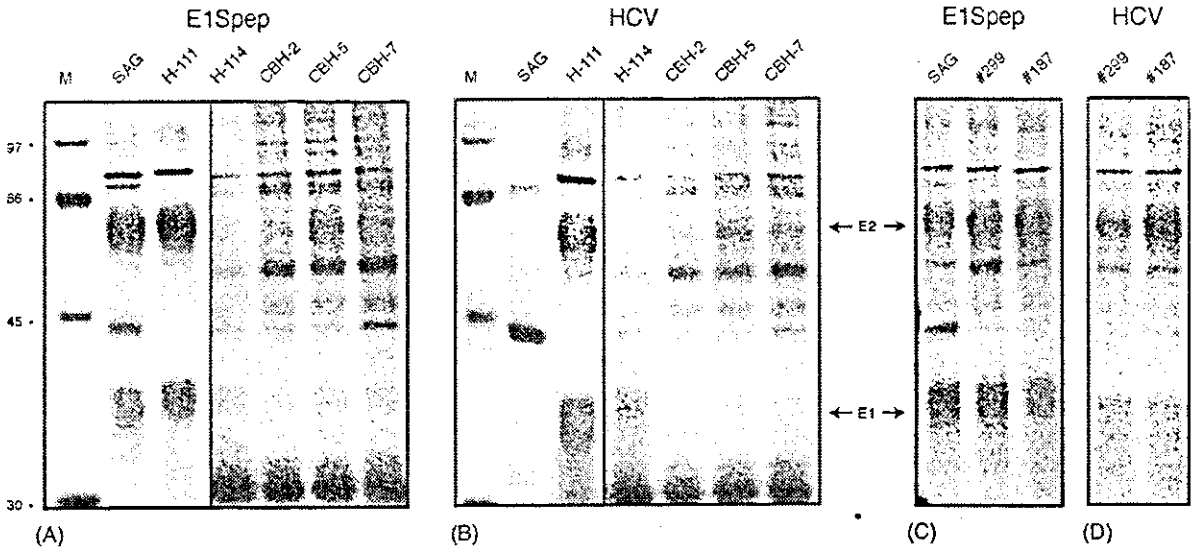

Fig. 5. Immunoprecipitation of E1–E2 complexes. Cells expressing the E1Spep (panels A and C) or the untagged HCV (panels B and D) polyprotein were metabolically labeled and lysed in solubilization buffer containing 1 mM DTT. Complexes were precipitated using the indicated reagents: SAG, human anti-E1 MAbs H-111 or H-114, human anti-E2 MAbs CBH-2, CBH-5 or CBH-7, or with murine anti-E1 MAb #299 or murine anti-E2 MAb #187. (A) Isolation of E1Spep-E2 complex using human MAbs. The image representing SAG and H-111 has been significantly lightened relative to that of the other human MAbs. Quantitation of radioactivity revealed that, relative to H-111, CBH-2 was able to precipitate 2% of the E2 glycoprotein, CBH-5 (13%), and CBH-7 (11%). Significant amounts were not detected using H-114. (B) Isolation of E1–E2 complex from untagged HCV polyprotein. Lanes representing SAG and H-111 are significantly lightened. Relative yields of E2 glycoprotein for CBH-5 and CBH-7 were 6 and 5%, respectively; no significant amounts of E2 were detected using H-114 or CBH-2. (C) and (D) Isolation of, respectively, E1Spep and HCV complex using murine MAbs #299 and #187.

3.3. Monoclonal antibodies as structural probes

To further assess the structural integrity of the noncovalently associated complex, we examined the ability of MAbs to recognize the solubilized glycoproteins. As depicted in Fig. 5, E1–E2 complex from cells expressing either the tagged or untagged HCV structural polyproteins was readily immunoprecipitated by murine MAbs directed against linear epitopes in either E1 or E2 (#299 and #187, respectively) and by the human anti-E1 MAb H-111. A significantly lesser amount of E1–E2 complex was isolated using conformation-dependent human MAbs directed to E1 (MAb H-114; Z.-Y. Keck and S.K.H. Foung, unpublished) or E2 (MAbs CBH-2, CBH-5 and CBH-7 (Hadlock et al., 2000; Triyatni et al., 2002)). Although these anti-E2 MAbs were isolated from a patient infected with a genotype 1b virus (Hadlock et al., 2000), we were able to recover at most 13% of the E1–E2 complex of this genotype 1b isolate. In other experiments, a similar pattern of reactivity was observed using complexes prepared in the absence of 1 mM DTT (data not shown). The overall diminution in reactivity of these human MAbs may be ascribed to antigenic differences between the virus of the MAb donor and those represented in the expression plasmid, or to conformational differences in the isolated complex. Importantly, however, the pattern of MAb reactivity was identical using complexes derived from the tagged and untagged HCV polyprotein. These parallels suggest that the immunochemical structure of the complex was not grossly perturbed by the introduction of the affinity tag.

Further attempts to ascertain the integrity of the complexes using a soluble form of the putative HCV receptor CD81 (Flint et al., 1999) were uninformative in that CD81 does not bind to genotype 1b glycoproteins (Roccasecca et al., 2003; Triyatni et al., 2002; Yagnik et al., 2000).

3.4. MAb binding to affinity-captured E1Spep–E2 complex and proteoliposomes

Taken together, our analyses suggested that assembly of the E1–E2 complex was largely unaffected by the introduction of the affinity tag at position 295/296 in E1. Based on computer predictions that the E1 glycoprotein may be able to adopt a polytopic topology in which the Spep-tagged region would lie on the cytoplasmic side of the membrane, we sought to reconstruct the predicted topology of the E1Spep glycoprotein by generating affinity-captured and properly oriented proteoliposomal complexes. We first used S-protein-conjugated paramagnetic beads to isolate E1Spep–E2 complex. Bound E1Spep was readily detected by flow cytometry using murine anti-E1 MAbs or the human MAbs H-111 (Fig. 6A) and associated E2 glycoprotein was demonstrated by Western blot analysis using the anti-E2 MAb #187 (Fig. 6B). The nonionic detergent was then replaced with a liposomal membrane to examine membrane topology. Because lipid accretion occurs at transmembrane regions of the bound proteins, continued exposure of E1 and E2 epitopes upon reconstitution would suggest that the ectodomains of E1 and E2 are properly oriented in the proteoliposome, despite anchoring by the affinity tag.

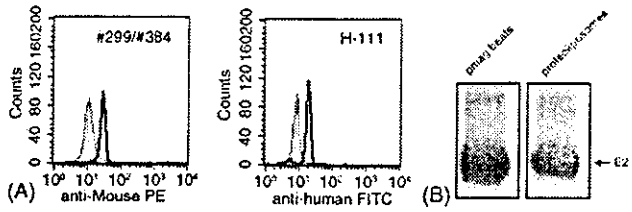

Fig. 6. Analysis of E1Spep and E2 glycoproteins on paramagnetic beads and proteoliposomes. S-protein coupled Dynabeads were used to isolate E1–E2 complex from lysates of cells expressing the E1Spep polyprotein. (A) Flow cytometric analysis of paramagnetic beads. Beads were incubated with anti-E1 MAbs in buffer containing 0.5% Cymal-5 nonionic detergent. Murine MAbs #299 and #384 (pooled) were detected using a second antibody labeled with phycoerythrin (PE); human MAb H-111 was detected using a second antibody labeled with fluorescein isothiocyanate (FITC). Histograms are shown in black lines. The negative control (filled, gray histograms) for the murine MAbs are paramagnetic beads bearing Spep-tagged CD4 (Gallina et al., 2002) and stained using the murine anti-E1 MAbs; the negative control for the human MAb are E1Spep paramagnetic beads stained using the anti-HIV MAb 447-52D (Conley et al., 1994). (B) Western blot analysis of E2 glycoprotein captured via E1Spep on paramagnetic beads (pmag beads) and subsequently retained in proteoliposomes. Lysates were prepared in solubilization buffer containing 1 mM DTT and bound E2 glycoprotein was detected using non-reducing SDS-PAGE and murine anti-E2 MAb #187.

Using protocols derived from Sodroski and colleagues (Babcock et al., 2001; Grundner et al., 2002; Mirzabekov et al., 2000), a mixture of synthetic lipids was added to the suspension of paramagnetic beads bearing the E1Spep–E2 complex, and the Cymal-5 nonionic detergent was then removed by dialysis to allow formation of the proteoliposomal membrane. Lipid accretion was sufficient to cover the paramagnetic bead, albeit not necessarily as a continuous membrane (see Section 2), and biochemical analysis of the reconstituted E1Spep–E2 proteoliposomes showed complete retention of the noncovalently associated E2 glycoprotein (Fig. 6B). Proteoliposomes constructed in this manner have, in many cases, been shown to display properly oriented and correctly folded glycoproteins (Grundner et al., 2002; Mirzabekov et al., 2000; Rigaud et al., 1995; Walter et al., 1990; CTM and JHN, unpublished).

Murine and human MAbs that recognized the detergent-solubilized E1Spep–E2 complex also recognized the proteoliposomal complex (Fig. 7). Linear epitopes within the E1 glycoprotein remained accessible to binding by murine MAbs #299 and #384, and #159 (kindly provided by J. Lau; (Triyatni et al., 2002)) and by the human anti-E1 MAb H-111. The retention of E1 glycoprotein exposure and reactivity, despite saturating amounts of lipid, is consistent with formation of the lipid bilayer between the ectodomain and the Spep anchor on the bead. Accretion of even a discontinuous bilayer at a single, C-terminal transmembrane domain would be anticipated to occlude antibody access to the now-buried ectodomain. In fact, binding to the proteoliposomes was comparable to that seen with the same paramagnetic beads prior to membrane accretion (see Fig. 6). The proteoliposomal E2 glycoprotein also remained accessible to murine MAb #187. As anticipated, little or no binding was detected using human MAbs that only weakly recognized the solubilized complexes (H-114, CBH-2, CBH-5 and CBH-7; Fig. 7).

Taken together, these studies suggest that the immunochemical properties of the E1Spep–E2 complex were unchanged by membrane reconstitution. These results are consistent with the prediction that E1 glycoprotein can assume a polytopic topology consisting of two membrane-spanning domains — the internal and C-terminal transmembrane regions — and an intervening cytoplasmic loop. In our studies with proteoliposomes, this topology was enforced by the Spep affinity tag. The parallel immune reactivity of the tagged and untagged glycoproteins in solution, however, suggests that the E1 glycoprotein may naturally display flexibility in its folding and membrane topology.

4. Discussion

Our studies suggest that the HCV E1 glycoprotein is able to adopt a polytopic topology in which the heterodimeric noncovalent association with the E2 glycoprotein subunit is retained. Further studies are clearly needed to prove the existence of this alternative form, and to define its relationship to the canonical, Type I form of the E1 glycoprotein. In the absence of a productive cell culture system for the growth of infectious HCV, direct links between envelope glycoprotein structure and function are difficult to demonstrate. In fact, a firm definition of the native structure(s) of the HCV envelope glycoproteins remains elusive despite the recent development of infectious pseudotyped virions bearing the E1–E2 complex (Bartosch et al., 2003; Drummer et al., 2003; Hsu et al., 2003). Nonetheless, our studies highlight the possibility that the E1 glycoprotein is capable of topologic flexibility.

In considering a cytoplasmic loop in the E1 glycoprotein (amino acids 285–344), it is perhaps significant that the potential glycosylation site at amino acid 325 is not utilized in the wild-type E1 glycoprotein (Meunier et al., 1999). Mutation to a more optimal glycosylation motif (NWSP to NTSG) enables only partial utilization of this site (Meunier et al., 1999). It is unclear whether the unglycosylated fraction reflects suboptimal glycosylation or a mixture of E1 topologies. Similarly, although the glycosylation site at position 305 appears to be utilized in some E1 glycoproteins (Meunier et al., 1999), this position is variably glycosylated in the genotype 1b isolate used here (YM, unpublished).

Topologic flexibility during biogenesis has been reported for other viral envelope glycoproteins. In the case of Hepatitis B virus, the surface glycoprotein is initially formed in the ER with the entire pre-S domain located in the cytosol; during maturation, 50% of the glycoprotein is converted to an alternative topology wherein the pre-S domain is translocated through the membrane to the lumenal side (Lambert and Prange, 2001 and references therein). Recently, Morri-

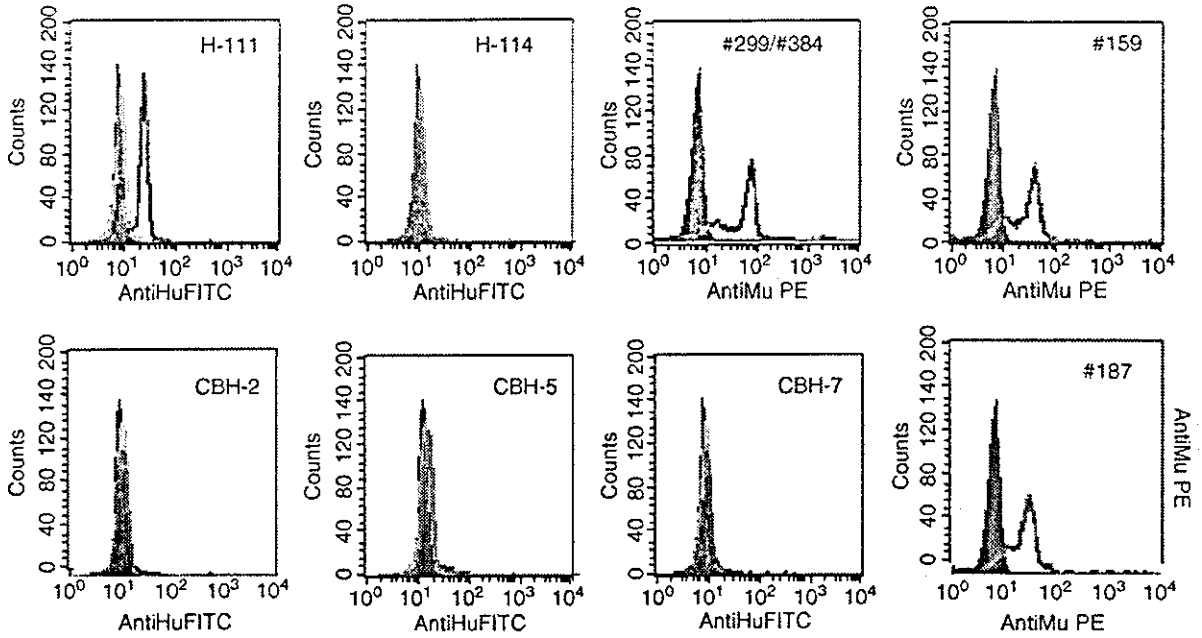

Fig. 7. Flow cytometric analysis of MAb binding to proteoliposomal E1–E2 complexes. Proteoliposomal beads were incubated with the indicated human or murine MAbs and subsequently stained using the appropriate secondary antibody conjugated, respectively, to FITC or PE. The murine anti-E1 MAb #159 was kindly provided by J. Lau (Triyatni et al., 2002). Control human MAbs directed to irrelevant antigens (HIV envelope glycoprotein gp120 and gp41, respectively) were kindly provided by S. Zolla-Pazner and M. Posner. A murine anti-gp41 MAb served as negative control for the murine anti-HCV MAbs and was kindly provided by G. Lewis. Histograms of anti-HCV MAb binding are shown by gray lines; control anti-HIV MAbs are shown in solid black histograms. For MAb H-111, the absence of binding to HIV-1 gp160 proteoliposomal beads (unpublished) is indicated in gray within the negative peak. The source of the minor, dull peak seen using the murine anti-HCV MAbs is unclear.

son and colleagues have reported that the fusion glycoprotein of Newcastle disease virus (NDV), for which a Type I membrane topology is well documented, can also assume a polytopic topology (McGinnes et al., 2003). The specific polytopic topology of the NDV fusion glycoprotein is similar to that which we propose for the HCV E1 glycoprotein.

If a cytoplasmic loop of E1 is involved in interactions with the virion core, as has been suggested (Lo et al., 1996; Merola et al., 2001), the immunochemical significance of an alternative form of the E1–E2 complex is unknown. In this regard, it is perhaps noteworthy that the human MAbs that weakly bind the E1–E2 complex in our studies have previously been described as broad in their specificity, recognizing determinants conserved between genotypes 1a and 1b (Hadlock et al., 2000). In other studies, however, gaps in this broad pattern of recognition have been observed (Cocquerel et al., 2003; Triyatni et al., 2002). The immunochemical differences noted in the literature may well be related to the genetic diversity among isolates or to the cell culture system used for recombinant expression. Based on our studies, we suggest that antigenic differences may also reflect the topologic flexibility of the HCV E1 glycoprotein. Although we cannot explain the apparent preference for the polytopic form in our studies, our findings raise the possibility that the topologic flexibility of the HCV E1 glycoprotein may play a role in immune evasion.

One might imagine that topologic flexibility in the E1–E2 complex could serve to direct the antibody response away from critical and conserved elements of the viral envelope spike. This concept has been best advanced in the case of the HIV envelope glycoprotein, where the antibody response is directed predominantly to variable epitopes displayed only on the monomeric gp120 subunit (Moore and Ho, 1995; Parren et al., 1997; Parren et al., 1999). Epitopes that give rise to rare broadly neutralizing anti-HIV MAbs appear to be physically and conformationally occluded within the oligomeric gp120–gp41 complex (Cao et al., 1997; Kwong et al., 2002; Saphire et al., 2001; Wyatt et al., 1995). By exposing antigenically variable determinants and minimizing conserved epitopes, HIV and HCV may be utilizing a common strategy, albeit via distinct mechanisms, to evade the immune response towards the establishment of chronic infection.

The task of designing an effective and much-needed HCV vaccine is complicated by the paucity of knowledge regarding the structure and function of the native HCV envelope glycoprotein complex. Recently, several laboratories have reported that infectious pseudotyped virions bearing the HCV E1–E2 complex can be generated in cell culture (Bartosch et al., 2003; Drummer et al., 2003; Hsu et al., 2003) and it is possible that this methodology may be refined to enable the biochemical and immunochemical dissection of the functional HCV envelope glycoprotein complex. In this regard, it may be important to consider the role of an alternative E1 glycoprotein topology in HCV biology and pathogenesis.

Acknowledgements

We thank Zhen-Yong Keck and Steven K. H. Foung (Stanford University) for providing human anti-E1 and anti-E2 MAbs and for valuable discussions throughout this project. Other reagents were kindly provided by S. Levy (Stanford University), J. Lau (Ribapharm), S. Zolla-Pazner (New York University), M. Posner (Harvard University) and G. Lewis (University of Maryland). This work was supported by the National Institutes of Health Grant R03 AI054388 to Jack H. Nunberg.

References

Abacioglu, Y.H., Fouts, T.R., Laman, J.D., Claassen, E., Pincus, S.H., Moore, J.P., Roby, C.A., Kamin-Lewis, R., Lewis, G.K., 1994. Epitope mapping and topology of baculovirus-expressed HIV-1 gp160 determined with a panel of murine monoclonal antibodies. AIDS Res. Hum. Retroviruses 10, 371–381.

Aizaki, H., Aoki, Y., Harada, T., Ishii, K., Suzuki, T., Nagamori, S., Toda, G., Matsuura, Y., Miyamura, T., 1998. Full-length complementary DNA of hepatitis C virus genome from an infectious blood sample. Hepatology 27, 621–627.

Babcock, G.J., Mirzabekov, T., Wojtowicz, W., Sodroski, J., 2001. Ligand-binding characteristics of CXCR4 incorporated into paramagnetic proteoliposomes. J. Biol. Chem. 276, 38,433–38,440.

Bartenschlager, R., Lohmann, V., 2001. Novel cell culture systems for the hepatitis C virus. Antiviral Res. 52, 1–17.

Bartosch, B., Dubuisson, J., Cosset, F.L., 2003. Infectious hepatitis C virus pseudo-particles containing functional E1–E2 envelope protein complexes. J. Exp. Med. 197, 633–642.

Cao, J., Sullivan, N., Desjardin, E., Parolin, C., Robinson, J., Wyatt, R., Sodroski, J., 1997. Replication and neutralization of human immunodeficiency virus type 1 lacking the V1 and V2 variable loops of the gp120 envelope glycoprotein. J. Virol. 71, 9808–9812.

Carrere-Kremer, S., Montpellier-Pala, C., Cocquerel, L., Wychowski, C., Penin, F., Dubuisson, J., 2002. Subcellular localization and topology of the p7 polypeptide of hepatitis C virus. J. Virol. 76, 3720–3730.

Cavacini, L.A., Emes, C.L., Wisnewski, A.V., Power, J., Lewis, G., Montefiori, D., Posner, M.R., 1998. Functional and molecular characterization of human monoclonal antibody reactive with the immunodominant region of HIV type 1 glycoprotein 41. AIDS Res. Hum. Retroviruses 14, 1271–1280.

Choukhi, A., Ung, S., Wychowski, C., Dubuisson, J., 1998. Involvement of endoplasmic reticulum chaperones in the folding of hepatitis C virus glycoproteins. J. Virol. 72, 3851–3858.

Cocquerel, L., Meunier, J.C., Pillez, A., Wychowski, C., Dubuisson, J., 1998. A retention signal necessary and sufficient for endoplasmic reticulum localization maps to the transmembrane domain of hepatitis C virus glycoprotein E2. J. Virol. 72, 2183–2191.

Cocquerel, L., Duvet, S., Meunier, J.C., Pillez, A., Cacan, R., Wychowski, C., Dubuisson, J., 1999. The transmembrane domain of hepatitis C virus glycoprotein E1 is a signal for static retention in the endoplasmic reticulum. J. Virol. 73, 2641–2649.

Cocquerel, L., Wychowski, C., Minner, F., Penin, F., Dubuisson, J., 2000. Charged residues in the transmembrane domains of hepatitis C virus glycoproteins play a major role in the processing, subcellular localization, and assembly of these envelope proteins. J. Virol. 74, 3623–3633.

Cocquerel, L., Op de Beeck, A., Lambot, M., Roussel, J., Delgrange, D., Pillez, A., Wychowski, C., Penin, F., Dubuisson, J., 2002. Topological changes in the transmembrane domains of hepatitis C virus envelope glycoproteins. EMBO J. 21, 2893–2902.

Cocquerel, L., Quinn, E.R., Flint, M., Hadlock, K.G., Foung, S.K., Levy, S., 2003. Recognition of native hepatitis C virus E1E2 heterodimers by a human monoclonal antibody. J. Virol. 77, 1604–1609.

Columbia University Bioinformatics Center, 2002. PredictProtein.

Conley, A.J., Gorny, M.K., Kessler II, J.A., Boots, L.J., Ossorio-Castro, M., Koenig, S., Lineberger, D.W., Emini, E.A., Williams, C., Zolla-Pazner, S., 1994. Neutralization of primary human immunodeficiency virus type 1 isolates by the broadly reactive anti-V3 monoclonal antibody, 447-52D. J. Virol. 68, 6994–7000.

Deleersnyder, V., Pillez, A., Wychowski, C., Blight, K., Xu, J., Hahn, Y.S., Rice, C.M., Dubuisson, J., 1997. Formation of native hepatitis C virus glycoprotein complexes. J. Virol. 71, 697–704.

Drummer, H.E., Maerz, A., Poumbourios, P., 2003. Cell surface expression of functional hepatitis C virus E1 and E2 glycoproteins. FEBS Lett. 546, 385–390.

Dubuisson, J., 2000. Folding, assembly and subcellular localization of hepatitis C virus glycoproteins. Curr. Top. Microbiol. Immunol. 242, 135–148.

Dubuisson, J., Hsu, H.H., Cheung, R.C., Greenberg, H.B., Russell, D.G., Rice, C.M., 1994. Formation and intracellular localization of hepatitis C virus envelope glycoprotein complexes expressed by recombinant vaccinia and Sindbis viruses. J. Virol. 68, 6147–6160.

Dubuisson, J., Rice, C.M., 1996. Hepatitis C virus glycoprotein folding: disulfide bond formation and association with calnexin. J. Virol. 70, 778–786.

Duvet, S., Cocquerel, L., Pillez, A., Cacan, R., Verbert, A., Moradpour, D., Wychowski, C., Dubuisson, J., 1998. Hepatitis C virus glycoprotein complex localization in the endoplasmic reticulum involves a determinant for retention and not retrieval. J. Biol. Chem. 273, 32,088–32,095.

Flint, M., Maidens, C., Loomis-Price, L.D., Shotton, C., Dubuisson, J., Monk, P., Higginbottom, A., Levy, S., McKeating, J.A., 1999. Characterization of hepatitis C virus E2 glycoprotein interaction with a putative cellular receptor, CD81. J. Virol. 73, 6235–6244.

Flint, M., McKeating, J.A., 1999. The C-terminal region of the hepatitis C virus E1 glycoprotein confers localization within the endoplasmic reticulum. J. Gen. Virol. 80, 1943–1947.

Gallina, A., Hanley, T.M., Mandel, R., Trahey, M., Broder, C.C., Viglianti, G.A., Ryser, H.J., 2002. Inhibitors of protein-disulfide isomerase prevent cleavage of disulfide bonds in receptor-bound glycoprotein 120 and prevent HIV-1 entry. J. Biol. Chem. 277, 50,579–50,588.

Grakoui, A., Wychowski, C., Lin, C., Feinstone, S.M., Rice, C.M., 1993. Expression and identification of hepatitis C virus polyprotein cleavage products. J. Virol. 67, 1385–1395.

Grundner, C., Mirzabekov, T., Sodroski, J., Wyatt, R., 2002. Solid-phase proteoliposomes containing human immunodeficiency virus envelope glycoproteins. J. Virol. 76, 3511–3521.

Hadlock, K.G., Lanford, R.E., Perkins, S., Rowe, J., Yang, Q., Levy, S., Pileri, P., Abrignani, S., Foung, S.K., 2000. Human monoclonal antibodies that inhibit binding of hepatitis C virus E2 protein to CD81 and recognize conserved conformational epitopes. J. Virol. 74, 10,407–10,416.

Hsu, M., Zhang, J., Flint, M., Logvinoff, C., Cheng-Mayer, C., Rice, C.M., McKeating, J.A., 2003. Hepatitis C virus glycoproteins mediate pH-dependent cell entry of pseudotyped retroviral particles. Proc. Natl. Acad. Sci. U. S. A. 100, 7271–7276.

Kim, J.-S., Raines, R.T., 1993. Ribonuclease S-peptide as a carrier in fusion proteins. Prot. Sci. 2, 348–356.

Kwong, P.D., Doyle, M.L., Casper, D.J., Cicala, C., Leavitt, S.A., Majeed, S., Steenbeke, T.D., Venturi, M., Chaiken, I., Fung, M., Katinger, H., Parren, P.W., Robinson, J., Van Ryk, D., Wang, L., Burton, D.R., Freire, E., Wyatt, R., Sodroski, J., Hendrickson, W.A., Arthos, J., 2002. HIV-1 evades antibody-mediated neutralization through conformational masking of receptor-binding sites. Nature 420, 678–682.

Lambert, C., Prange, R., 2001. Dual topology of the hepatitis B virus large envelope protein: determinants influencing post-translational pre-S translocation. J. Biol. Chem. 276, 22,265–22,272.

Lin, C., Lindenbach, B.D., Pragai, B.M., McCourt, D.W., Rice, C.M., 1994. Processing in the hepatitis C virus E2-NS2 region: identification of p7 and two distinct E2-specific products with different C termini. J. Virol. 68, 5063–5073.

Lo, S.Y., Selby, M.J., Ou, J.H., 1996. Interaction between hepatitis C virus core protein and E1 envelope protein. J. Virol. 70, 5177–5182.

Lu, M., Stoller, M.O., Wang, S., Liu, J., Fagan, M.B., Nunberg, J.H., 2001. Structural and functional analysis of interhelical interactions in the HIV-1 gp41 envelope glycoprotein by alanine-scanning mutagenesis. J. Virol. 75, 11,146–11,156.

Matsuura, Y., Suzuki, T., Suzuki, R., Sato, M., Aizaki, H., Saito, I., Miyamura, T., 1994. Processing of E1 and E2 glycoproteins of hepatitis C virus expressed in mammalian and insect cells. Virology 205, 141–150.

McGinnes, L.W., Reitter, J.N., Gravel, K., Morrison, T.G., 2003. Evidence for mixed membrane topology of the Newcastle disease virus fusion protein. J. Virol. 77, 1951–1963.

Merola, M., Brazzoli, M., Cocchiarella, F., Heile, J.M., Helenius, A., Weiner, A.J., Houghton, M., Abrignani, S., 2001. Folding of hepatitis C virus E1 glycoprotein in a cell-free system. J. Virol. 75, 11,205–11,217.

Meunier, J.C., Fournillier, A., Choukhi, A., Cahour, A., Cocquerel, L., Dubuisson, J., Wychowski, C., 1999. Analysis of the glycosylation sites of Hepatitis C virus (HCV) glycoprotein E1 and the influence of E1 glycans on the formation of the HCV glycoprotein complex. J. Gen. Virol. 80, 887–896.

Michalak, J.P., Wychowski, C., Choukhi, A., Meunier, J.C., Ung, S., Rice, C.M., Dubuisson, J., 1997. Characterization of truncated forms of hepatitis C virus glycoproteins. J. Gen. Virol. 78, 2299–2306.

Mirzabekov, T., Kontos, H., Farzan, M., Marasco, W., Sodroski, J., 2000. Paramagnetic proteoliposomes containing a pure, native, and oriented seven-transmembrane segment protein, CCR5. Nat. Biotech. 18, 649–654.

Mizushima, H., Hijikata, M., Asabe, S., Hirota, M., Kimura, K., Shimotohno, K., 1994. Two hepatitis C virus glycoprotein E2 products with different C termini. J. Virol. 68, 6215–6222.

Moore, J.P., Ho, D.D., 1995. HIV-1 neutralization: the consequences of viral adaptation to growth on transformed T cells. AIDS 9 (Suppl. A), S117–S136.

Op De Beeck, A., Montserret, R., Duvet, S., Cocquerel, L., Cacan, R., Barberot, B., Le Maire, M., Penin, F., Dubuisson, J., 2000. The transmembrane domains of hepatitis C virus envelope glycoproteins E1 and E2 play a major role in heterodimerization. J. Biol. Chem. 275, 31,428–31,437.

Op De Beeck, A., Cocquerel, L., Dubuisson, J., 2001. Biogenesis of hepatitis C virus envelope glycoproteins. J. Gen. Virol. 82, 2589–2595.

Parren, P.W., Gauduin, M.C., Koup, R.A., Poignard, P., Sattentau, Q.J., Fisicaro, P., Burton, D.R., 1997. Relevance of the antibody response against human immunodeficiency virus type 1 envelope to vaccine design. Immunol. Lett. 58, 125–132.

Parren, P.W.H.I., Moore, J.P., Burton, D.R., Sattentau, Q.J., 1999. The neutralizing antibody response to HIV-1: viral evasion and escape from humoral immunity. AIDS 13 (Suppl. A), S137–S162.

Patel, J., Patel, A.H., McLauchlan, J., 2001. The transmembrane domain of the hepatitis C virus E2 glycoprotein is required for correct folding of the E1 glycoprotein and native complex formation. Virology 279, 58–68.

Reed, K.E., Rice, C.M., 2000. Overview of hepatitis C virus genome structure, polyprotein processing, and protein properties. Curr. Top. Microbiol. Immunol. 242, 55–84.

Richards, F.M., Vithayathil, P.J., 1959. The preparation of subtilisin-modified ribonuclease and the separation of the peptide and protein components. J. Biol. Chem. 234, 1459–1465.

Rigaud, J.L., Pitard, B., Levy, D., 1995. Reconstitution of membrane proteins into liposomes: application to energy-transducing membrane proteins. Biochem. Biophys. Acta 1231, 223–246.

Roccasecca, R., Ansuini, H., Vitelli, A., Meola, A., Scarselli, E., Acali, S., Pezzanera, M., Ercole, B.B., McKeating, J., Yagnik, A., Lahm, A., Tramontano, A., Cortese, R., Nicosia, A., 2003. Binding of the hepatitis C virus E2 glycoprotein to CD81 is strain specific and is modulated by a complex interplay between hypervariable regions 1 and 2. J. Virol. 77, 1856–1867.

Rost, B., Casadio, R., Fariselli, P., Sander, C., 1995. Transmembrane helices predicted at 95% accuracy. Prot. Sci. 4, 521–533.

Saphire, E.O., Parren, P.W., Pantophlet, R., Zwick, M.B., Morris, G.M., Rudd, P.M., Dwek, R.A., Stanfield, R.L., Burton, D.R., Wilson, I.A., 2001. Crystal structure of a neutralizing human IGG against HIV-1: a template for vaccine design. Science 293, 1155–1159.

Selby, M.J., Choo, Q.L., Berger, K., Kuo, G., Glazer, E., Eckart, M., Lee, C., Chien, D., Kuo, C., Houghton, M., 1993. Expression, identification and subcellular localization of the proteins encoded by the hepatitis C viral genome. J. Gen. Virol. 74, 1103–1113.

Takikawa, S., Ishii, K., Aizaki, H., Suzuki, T., Asakura, H., Matsuura, Y., Miyamura, T., 2000. Cell fusion activity of hepatitis C virus envelope proteins. J. Virol. 74, 5066–5074.

Tatu, U., Braakman, I., Helenius, A., 1993. Membrane glycoprotein folding, oligomerization and intracellular transport: effects of dithiothreitol in living cells. EMBO J. 12, 2151–2157.

Triyatni, M., Vergalla, J., Davis, A.R., Hadlock, K.G., Foung, S.K., Liang, T.J., 2002. Structural features of envelope proteins on hepatitis C virus-like particles as determined by anti-envelope monoclonal antibodies and CD81 binding. Virology 298, 124–132.

von Heijne, G., 1988. Transcending the impenetrable: how proteins come to terms with membranes. Biochim. Biophys. Acta 947, 307–333.

Walter, A., Eidelman, O., Ollivon, M., Blumenthal, R., 1990. Functional reconstitution of viral envelopes. In: "Membrane Fusion" Wilschut, J., Hoekstra, D. (Eds.), Marcel Dekker, Inc., pp. 395–418.

World Health Organization, 1999. Global surveillance and control of hepatitis C. J. Viral Hepatitis 6, 35–47.

Wyatt, R., Moore, J.P., Accola, M., Desjardin, E., Robinson, J., Sodroski, J., 1995. Involvement of the V1/V2 variable loop structure in the exposure of human immunodeficiency virus type 1 gp120 epitopes induced by receptor binding. J. Virol. 69, 5723–5733.

Yagnik, A.T., Lahm, A., Meola, A., Roccasecca, R.M., Ercole, B.B., Nicosia, A., Tramontano, A., 2000. A model for the hepatitis C virus envelope glycoprotein E2. Proteins 40, 355–366.

International Immunology, Vol. 16, No. 10, pp. 1423–1430
doi:10.1093/intimm/dxh143 Advance Access publication 16 August 2004

A subcutaneously injected UV-inactivated SARS coronavirus vaccine elicits systemic humoral immunity in mice

Naomi Takasuka[1], Hideki Fujii[1], Yoshimasa Takahashi[1], Masataka Kasai[1], Shigeru Morikawa[2], Shigeyuki Itamura[4], Koji Ishii[3], Masahiro Sakaguchi[1], Kazuo Ohnishi[1], Masamichi Ohshima[1], Shu-ichi Hashimoto[1], Takato Odagiri[4], Masato Tashiro[4], Hiroshi Yoshikura[5], Toshitada Takemori[1] and **Yasuko Tsunetsugu-Yokota[1]**

[1]Department of Immunology, [2]First, [3]Second and [4]Third Departments of Virology, [5]National Institute of Infectious Diseases, Toyama 1-23-1, Shinjuku-ku, Tokyo 162-8640, Japan

Keywords: alum, cellular immunity, neutralizing antibody, parenteral administration, vaccination

Abstract

The recent emergence of severe acute respiratory syndrome (SARS) was caused by a novel coronavirus, SARS-CoV. It spread rapidly to many countries and developing a SARS vaccine is now urgently required. In order to study the immunogenicity of UV-inactivated purified SARS-CoV virion as a vaccine candidate, we subcutaneously immunized mice with UV-inactivated SARS-CoV with or without an adjuvant. We chose aluminum hydroxide gel (alum) as an adjuvant, because of its long safety history for human use. We observed that the UV-inactivated SARS-CoV virion elicited a high level of humoral immunity, resulting in the generation of long-term antibody secreting and memory B cells. With the addition of alum to the vaccine formula, serum IgG production was augmented and reached a level similar to that found in hyper-immunized mice, though it was still insufficient to elicit serum IgA antibodies. Notably, the SARS-CoV virion itself was able to induce long-term antibody production even without an adjuvant. Anti-SARS-CoV antibodies elicited in mice recognized both the spike and nucleocapsid proteins of the virus and were able to neutralize the virus. Furthermore, the UV-inactivated virion induced regional lymph node T-cell proliferation and significant levels of cytokine production (IL-2, IL-4, IL-5, IFN-γ and TNF-α) upon restimulation with inactivated SARS-CoV virion *in vitro*. Thus, a whole killed virion could serve as a candidate antigen for a SARS vaccine to elicit both humoral and cellular immunity.

Introduction

A new disease called severe acute respiratory syndrome (SARS) originated in China in late 2002 and spread rapidly to many countries. Upon this outbreak, a global collaboration network was coordinated by WHO. As a result of this unprecedented international effort, a novel type of coronavirus (SARS-CoV) was identified as the etiologic agent of SARS (1,2) in March 2003. The genomic sequence of SARS-CoV was completed and we now know that SARS-CoV has all the features and characteristics of other coronaviruses, but it is quite different from all previously known coronaviruses (groups I–III), representing a new group (group IV) (3,4). It is assumed that SARS-CoV is a mutant coronavirus transmitted from a wild animal that developed the ability to productively infect humans (3,5). The genome of SARS-CoV is a single-stranded plus-sense RNA ~30 kb in length and containing five major open reading frames that encode non-structural replicase polyproteins and structural proteins: the spike (S), envelope (E), membrane (M) and nucleocapsid protein (N), in the same order and of approximately the same sizes as those of other coronaviruses (5).

The reason why SARS-CoV induces severe respiratory distress in some, but not all, infected individuals is still unclear. In patients with SARS and probable SARS cases, virus is detected in sputum, stool and plasma by RT–PCR (1,2). These patients developed serum antibodies against SARS-CoV and high antibody titers against N protein were maintained for more than 5 months after infection (6). Because of their generally poor pathogenicity and difficulty of propagation

Correspondence to: Y. Tsunetsugu-Yokota; E-mail: yyckota@nih.go.jp

Transmitting editor: K. Sugamura

Received 6 May 2004, *accepted* 15 July 2004

in vitro, there have been few studies regarding immunity to human coronaviruses OC43 and 229E. In the veterinary field, however, coronaviruses have been known for many years to cause a variety of lung, liver and gut diseases in animals. As we learned from these animal models, both humoral and cellular immune responses may contribute to protection against coronavirus diseases, including SARS [for review see (7)].

The clinical manifestation of SARS is hardly distinct from other common respiratory viral infections including influenza. Because an influenza epidemic may occur simultaneously with the re-emergence of SARS, it is urgently required that we develop effective SARS vaccines as well as sensitive diagnostic tests specific for SARS. Recently, the angiotensin-converting enzyme 2 (ACE2) was identified as a cellular receptor for SARS-CoV (8). The first step in viral infection is presumably the binding of S protein to its receptor, ACE2. In the murine MHV model, S proteins are known to contain important virus-neutralizing epitopes that elicit neutralizing antibodies in mice (9,10). Therefore, the S protein would be the first candidate coronavirus protein for induction of immunity. However, the S, M and N proteins are also known to contribute to generating the host immune response (11,12).

Following an established vaccine protocol is one of the best ways to shorten the time and cost of new vaccine development. Most of the currently available vaccines for humans are inactivated and applied cutaneously, except oral polio vaccine, and adjuvant usage is mostly limited to aluminum hydroxide gel (alum). In order to know the immunogenicity of inactivated SARS-CoV as a vaccine candidate, we immunized mice with UV-inactivated SARS-CoV either with or without alum. We report here the evaluation of humoral and cellular immunity elicited by UV-inactivated SARS-CoV administered subcutaneously.

Methods

Preparation of UV-inactivated purified SARS-CoV

SARS-CoV (HKU39849) was kindly supplied by Dr J.S.M. Peiris, Department of Microbiology, The University of Hong Kong. The virus was amplified in Vero E6 cells and purified by sucrose density gradient centrifugation. Concentrated virus was then exposed to UV light (4.75 J/cm^2) in order to inactivate the virus. We confirmed that the virus completely lost its infectivity by this method.

Immunization of mice

Female BALB/c mice were purchased from Nippon SLC Inc. (Shizuoka, Japan) and were housed under specific pathogen-free conditions. All experimental procedures were carried out under NIID-recommended guidelines. Mice were subcutaneously injected via their back or right and left hind leg footpads with 10 μg of UV-inactivated purified SARS-CoV with or without 2 mg of alum, and boosted by the same procedure 7 weeks after priming.

Detection of immunoglobulins in the serum samples

Blood was obtained from the tail vein and allowed to clot overnight at 4°C. Sera were then collected by centrifugation. For ELISA, microtiter plates (Dynatech, Chantily, VA) were coated overnight at 4°C with SARS-CoV-infected or mock-infected Vero E6 cell lysates, which had been treated with 1% NP40 followed by UV-inactivation. To detect S or N protein, the plates were coated with 1% NP40 lysates of chick embryo fibroblasts that had been infected with S or N protein-expressing DIs (attenuated vaccinia virus) (13). The plates were blocked with 1% OVA in PBS–Tween (0.05%) and then incubated with the sera serially diluted at 1:25–1:10^5 for 1 h at room temperature. Plates were incubated with either peroxidase-conjugated anti-mouse IgG (1:2000, Zymed, San Francisco, CA), IgM or IgA (1:2000, Southern Biotechnology, Birmingham, AL) antibody. For detection of IgG subclasses, either peroxidase-conjugated anti-mouse IgG_1, IgG_{2a}, IgG_{2b} (1:2000, Zymed) or IgG_3 (1:2000, Southern Biotechnology) was used. Plates were washed three times with PBS–Tween at each step. Antibodies were detected by *O*-phenylenediamine (Zymed), and the absorbance of each well was read at 490 nm using a model 680 microplate reader (Bio-Rad, Hercules, CA). As a standard for IgG detection, serum was obtained from a hyper-immunized mouse; the OD490nm value of 100 U/ml standard was ~3 in all assays. SARS-CoV-specific IgG titer was calculated as follows: SARS-specific IgG titer (U/ml) = (the unit value obtained at wells coated with virus-infected cell lysates) – (the unit value obtained at wells coated with non-infected cell lysates).

ELISPOT assay for antibody-secreting cells (ASCs)

Recombinant N protein (amino acids 1–49 and 340–390) of SARS-CoV (Biodesign, Saco, ME) was diluted to 10 μg/ml in PBS, and then added at 100 μl per well to plates supported by a nitrocellulose filter (Millipore, Bedford, MA). After overnight incubation at 4°C, the plates were washed with PBS three times and then blocked at 4°C overnight with 1% OVA in PBS–Tween (0.05%). After erythrocyte lysis, single cell suspensions from BMs were suspended in RPMI supplemented with 10% FCS, 5 × 10^{-5} M 2ME, 2 mM L-glutamine, 100 U/ml penicillin and 100 μg/ml streptomycin, and then applied to the plates at a concentration of 3 × 10^5 cells per well. After 24 h cultivation, the plates were recovered and stained with alkaline phosphatase-conjugated anti-mouse IgG_1 antibody (Southern Biotechnologies). Alkaline phosphatase activity was visualized using 3-amino-ethyl carbozole and napthol AS-MX phosphate/fast blue BB (Sigma). The frequency of plasma cells specific for N protein was determined from the N protein-coated plates after background on the uncoated plates was subtracted.

Coronavirus neutralizing assay

Serum was inactivated by incubation at 56°C for 30 min. The known tissue culture infectious dose (TCID) of SARS-CoV was incubated for 1 h in the presence or absence of serum antibodies serially diluted 5-fold, and then added to Vero E6 cell culture grown confluently in a 96-well microtiter plate. After 48 h, cells were fixed with 10% formaldehyde and stained with crystal violet to visualize the cytopathic effect induced by the virus (14). Neutralization antibody titers were expressed as the minimum dilution number of serum that inhibited the cytopathic effect.

Western blotting

Purified SARS-CoV virion (0.5 μg) was fractionated on SDS-PAGE under reduced conditions. Proteins were transferred to PVDF membrane (Genetics, Tokyo, Japan) and reacted with the diluted sera (1:1000) that had been obtained from mice inoculated with UV-irradiated SARS-CoV. After washing, the membrane was reacted with HRP-conjugated $F(ab')_2$ fragment anti-mouse IgG (H+L) (1:20 000 Jackson Immuno Research, West Grove, PA), followed by visualization of the bands on X-ray film (Kodak, Rochester, NY) using chemiluminescent regents (Amasham Biosciences, Piscataway, NJ).

Regional T cell response

Popliteal and inguinal lymph nodes and spleens were harvested from mice 1 week after the boost vaccination. After the preparation of a single cell suspension, T cells were purified by depletion of $B220^+$, $Gr1^+$, $CD11b^+$, IgD^+ and IgM^+ cells using a magnetic cell sort system (MACS: Miltenyi Biotec, Bergisch Gladbach, Germany). To prepare antigen-presenting cells (APC), normal BALB/c mouse splenocytes were depleted of $CD3^+$ T cells by MACS and irradiated at 2000 cGy.

Purified T cells taken from lymph nodes (1×10^5 cells/well) were cultured with irradiated APC (5×10^5 cells/well) in the presence or absence of UV-irradiated purified SARS-CoV virion (1 or 10 μg/ml). Four days after the cultivation, the level of cytokine concentration in the culture supernatant was measured by flow cytometry using a mouse Th1/Th2 cytokine cytometric bead array kit (Becton Dickinson, San Jose, CA). T-cell proliferation was monitored by the incorporation of [^{3}H]thymidine (18.5 kBq/well, ICN Biomedicals, Costa Mesa, CA) added 8 h prior to cell harvest. The cells were harvested on a 96-well microplate bonded with a GF/B filter (Packard Instruments, Meriden, CT). Incorporated radioactivity was counted by a microplate scintillation counter (Packard Instruments).

Results

Inoculation with UV-inactivated SARS-CoV results in an antigen-specific IgG_1 response, probably by generating long-term ASCs as well as memory cells

To examine the level of anti-SARS-CoV response in mice after inoculation with vaccine candidates, three mice in each group were subcutaneously inoculated with 10 μg of UV-inactivated purified SARS-CoV with (Virion/Alum) or without alum (Virion), or inoculated with alum alone (Alum) or left untreated (None) as a control (Fig. 1). One month after inoculation, vaccinated mice elicited the anti-SARS CoV IgG antibody in sera at high levels. As expected, the alum adjuvant enhanced the level of IgG antibody response, >10-fold higher than the level without adjuvant (Fig. 1C compared with B). When mice were boosted at 7 weeks, the level of IgG antibody in both groups of mice was further increased ~10-fold above the primary response (Fig. 1B and C). Notably, the level of serum antibodies induced by a single injection of virion, even in the absence of the alum adjuvant, was maintained at least more than 6 months (Fig. 1D). These results suggest that long-term ASCs can be established by a single shot of UV-inactivated virion administration.

Upon restimulation with antigen, memory B cells rapidly differentiate into ASCs and migrate into the bone marrow to establish a long-term ASC pool (15,16). To enumerate the number of plasma cells specific for SARS-CoV, we performed an ELISPOT assay using recombinant N proteins, amino acid numbers 1–49 (N1–49) and 340–390 (N340–390) as coating antigens. Consistent with the serum anti-SARS CoV IgG level, SARS-specific IgG_1 plasma cells were maintained in the bone marrow at day 10 after boost immunization with virion/alum

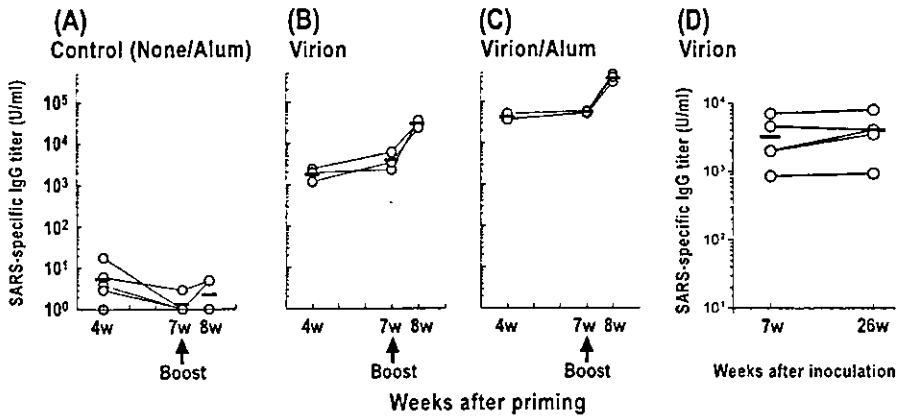

Fig. 1. The level of SARS-specific IgG in subcutaneously vaccinated mice. Mice were subcutaneously primed with 10 μg of UV-inactivated SARS-CoV virion (B), or virion with 2 mg of alum (C), or alum alone or none (A) and boosted with the same dose in their footpads at 7 weeks after priming. Serum was collected at the indicated time point and subjected to ELISA to detect SARS-specific IgG using SARS-CoV-infected Vero cell lysates as a coating antigen. Circles and bars represent the amount of IgG antibody in the serum of each mouse and the mean, respectively. The amount of IgG was arbitrarily calculated based on the concentration of hyper-immune sera. A representative result of two independent experiments is shown. (D) Mice were vaccinated with 10 μg of UV-inactivated SARS-CoV virion subcutaneously into their backs. Serum was collected from individual mice at the indicated time point and subjected to ELISA to detect SARS-specific IgG.

(Fig. 2). In contrast, the number of spots from control mice was below the detection limit (i.e. <1 ASC/9 × 10^5 cells).

UV-inactivated SARS-CoV induces IgG_1 antibody with neutralizing activity

We determined the subclass of serum anti-SARS-CoV IgG antibodies in the boosted mice using anti-mouse IgG_1, IgG_{2a}, IgG_{2b} or IgG_3 second antibody by ELISA (Fig. 3). Interestingly, the level of anti-SARS-CoV IgG_{2a} in mice immunized with virion/alum was comparable to that in mice immunized with virion alone, whereas the level of anti-SARS-CoV IgG_1 was higher in mice with virion/alum than the mice with virion alone. In contrast, the levels of IgG_{2b} and IgG_3 antibodies were fairly low in both groups. Therefore, our results indicated that vaccination with a combination of inactivated virion and alum induced a predominantly Th2-type immune response.

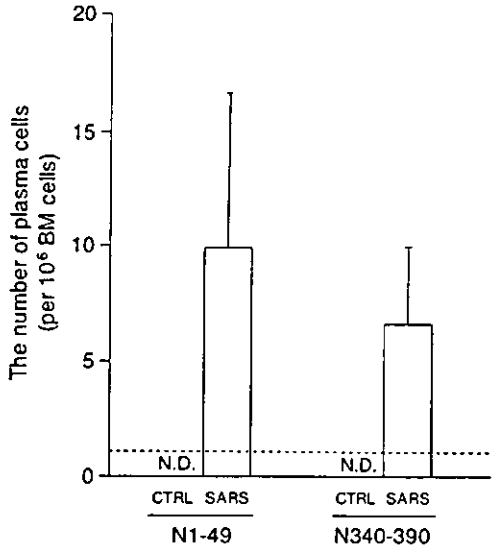

Fig. 2. The number of SARS-specific IgG_1 plasma cells in BM. Mice were primed and boosted by subcutaneous injection into their back with 10 μg of UV-inactivated SARS-CoV virion with 2 mg of alum (VA). BMs were collected at 10 days after boost and subjected to ELISPOT to detect SARS-specific IgG_1 plasma cells. Bars represent the number of plasma cells specific to N1–49 and N340–390 antigen in SARS-vaccinated and control mice, respectively. Data are means of triplicate cultures. The number of spots from control mice was below the detection limit (i.e. <1 ASC/9 × 10^5 cells: dashed line). A representative result of two independent experiments is shown. N.D.: not detected.

We also measured serum immunoglobulins other than IgG in the early and late phases of immunization. To avoid high IgG concentrations interfering with the detection of IgM and IgA antibodies, the serum IgG was absorbed with protein G-conjugated beads (>98%). The levels of anti-SARS-CoV IgM antibodies in the IgG-depleted sera, which were obtained 4 weeks after priming, were below our detection limit. Likewise, anti-SARS-CoV IgA antibody in the IgG-depleted sera, which were obtained 1 week after booster, was not detectable (data not shown).

Whether or not immune sera possess a neutralizing activity against SARS-CoV is a crucial aspect of vaccination. We estimated the neutralizing activity of sera obtained 1 week after boost inoculation (Table 1). We observed that neutralizing activity against SARS-CoV was detected at a high level in sera of mice inoculated with virion/alum or virion alone. Taken together, these results indicate that subcutaneous vaccination with UV-inactivated SARS-CoV virion is able to elicit a sufficient amount of IgG antibodies with neutralizing activity.

UV-inactivated SARS-CoV induces serum IgG antibody specific for S and N proteins

Using the immune sera of mice boosted with virion/alum 1 week before, we analyzed the specificity of serum IgG by western blot analysis (see Methods). As shown in Fig. 4(A), the robust signal detected at 50 kDa corresponds to the N protein of SARS-CoV, as predicted by its genome size (3,4). A band near 200 kDa appears to correspond to S protein, analogous with the S protein of other human coronaviruses, HCV-229E

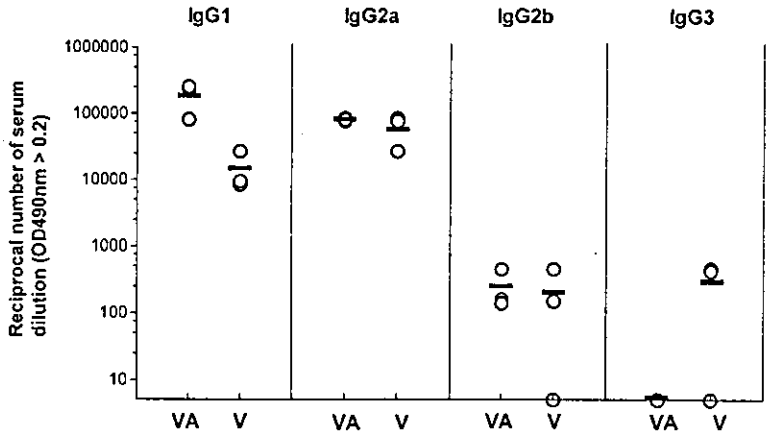

Fig. 3. IgG subclass of immunized serum. Mice were subcutaneously primed and boosted by injection in their footpads with 10 μg of UV-inactivated SARS-CoV virion (V), or virion with 2 mg of alum (VA). Serum was collected from individual mice at 1 week after boost and subjected to ELISA to detect SARS-specific IgG_1, IgG_{2a}, IgG_{2b} and IgG_3 titer. The Y value is the reciprocal serum dilution number where the OD490nm ≥ 0.2 in each ELISA. Circles and bars represent the titer for each mouse and the mean, respectively; results are representative of two separate experiments.

and HCV-OC43, which are known to be heavily glycosylated and detected at 186 kDa and 190 kDa, respectively (17). Our result is consistent with the data reported recently by Xiao *et al.* who expressed the full-length S glycoprotein of SARS-CoV Tor2 strain in 293 cells and showed that the protein ran ~180–200 kDa in SDS gels (18). The origins of the 120 kDa and the faint 37 kDa bands were unknown. However, similar bands were also detected on a fluorogram by using anti-N mAbs (Onnishi, K., Sakaguchi, M., Takasuka, N. *et al.*, unpublished data), suggesting that it is related to N protein. The specificity of IgG in the immune sera was also determined by ELISA plates coated with lysates of cells infected with either S- or N-expressing recombinant vaccinia viruses (Fig. 4B). The results indicated that anti-S as well as anti-N protein IgG antibodies were elicited by virion/alum vaccination.

Table I. Neutralizing activity in serum after vaccination

		Reciprocal endpoint titer	
		Experiment 1	Experiment 2
None/alum		<5*	<5*
Virion	mouse 1	250	250
	2	1250	250
	3	1250	250
Virion/alum	1	250	1250
	2	1250	1250
	3	1250	1250

*All six mice examined did not have detectable neutralizing activity. Sera were obtained from mice 1 week after boost vaccination and subjected to SARS-CoV neutralizing activity assay as described in Methods. The titer is a reciprocal number of minimum serum dilution that inhibits the cytopathic effect.

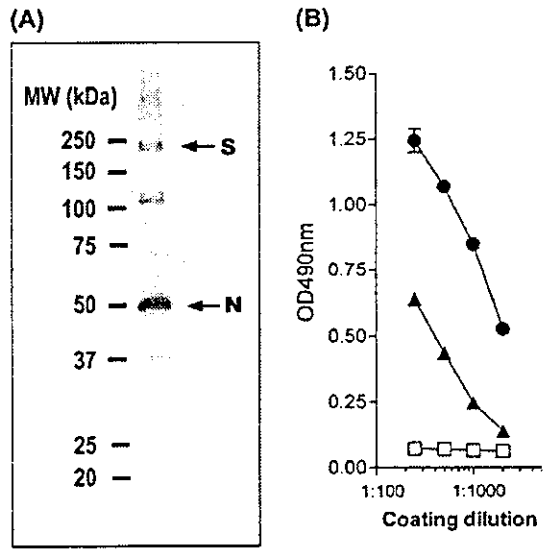

Fig. 4. Specificity of the serum antibodies. (A) Purified UV-inactivated SARS-CoV virion (0.5 μg) was fractionated by SDS–PAGE and subjected to western blotting. Diluted pooled sera (1:1000) from mice primed and boosted with virion/alum were exploited to detect virus proteins. Upper and lower arrows indicate the predicted band of S (spike protein) and N (nucleocapside protein) of SARS-CoV, respectively. The size of molecular weight markers (kDa) is shown on the left. (B) S protein- or N protein-specific ELISA. ELISA plates were coated at the indicated dilution with 1% NP40 lysates of chick embryo fibroblasts that had been infected with S protein-expressing vaccinia virus (circle), N protein-expressing vaccinia virus (triangle) or uninfected (mock; square). Diluted serum (1:1000) from mice prime and boost immunized with virion/alum, was exploited for detection of virus proteins.

UV-inactivated SARS-CoV whole virion induces T-cell response

To examine whether or not subcutaneously vaccinated mice gained an induced T-cell response against SARS-CoV, mice were immunized either with virion/alum, virion, or alum only via the footpad. T cells of these mice were enriched from the spleen and regional lymph nodes 1 week after a booster immunization and cultured with irradiated APCs in the presence or absence of UV-inactivated SARS-CoV virion at 1 or 10 μg/ml. As shown in Fig. 5(A), regional lymph node T cells proliferated *in vitro* in response to UV-inactivated virion in virion/alum-immunized mice and, to a lesser extent, in virion-immunized mice. Because mice inoculated with virion/alum showed a high basal level of proliferation of lymph node T cells in the absence of antigen, there is not much difference in the net proliferative response of these cells between the virion/alum group and the virion only group. On the other hand, in splenic T cells, a low level of proliferation was observed only in the virion/alum group of mice. The level of proliferation of these T cells, however, was virion-dose independent. Therefore, our results suggest that the subcutaneous injection of inactivated virion, even without alum, does induce T cell activation to some extent in the draining lymph node, a result which hardly occurs systemically.

We also measured the level of cytokine production in the supernatant of lymph node T cells stimulated with inactivated virion *in vitro* for 4 days. We found that the inactivated virion induced the production of all the cytokines (IL-2, IL-4, IL-5, IFN-γ and TNF-α) in T cells of virion/alum-immunized mice, in a dose-dependent manner (Fig. 5B). Likewise, T cells of virion-immunized mice produced low, yet significant, levels of these cytokines in a dose-dependent manner, except IL-5. In contrast, lymph node T cells from normal mice did not produce any cytokines at all in response to virion, suggesting that the virion itself does not possess innate stimulating activity as bacterial products [such as lipopolysaccharide (LPS) and purified protein derivative of mycobacterium tuberculosis (PPD)] do. Taken together, these results suggest that subcutaneous vaccination with UV-inactivated SARS-CoV is able to activate $CD4^+$ T cells in regional lymph nodes, where T cells produce several immunoregulatory cytokines, including IFN-γ.

Discussion

The present results demonstrated that even a single subcutaneous administration of UV-irradiated virion without alum adjuvant induced a high level of systemic anti-SARS-CoV antibody response in mice, probably followed by the generation of long-term antibody-secreting cells and memory cells in the bone marrow. Considering that polyvalent particulate

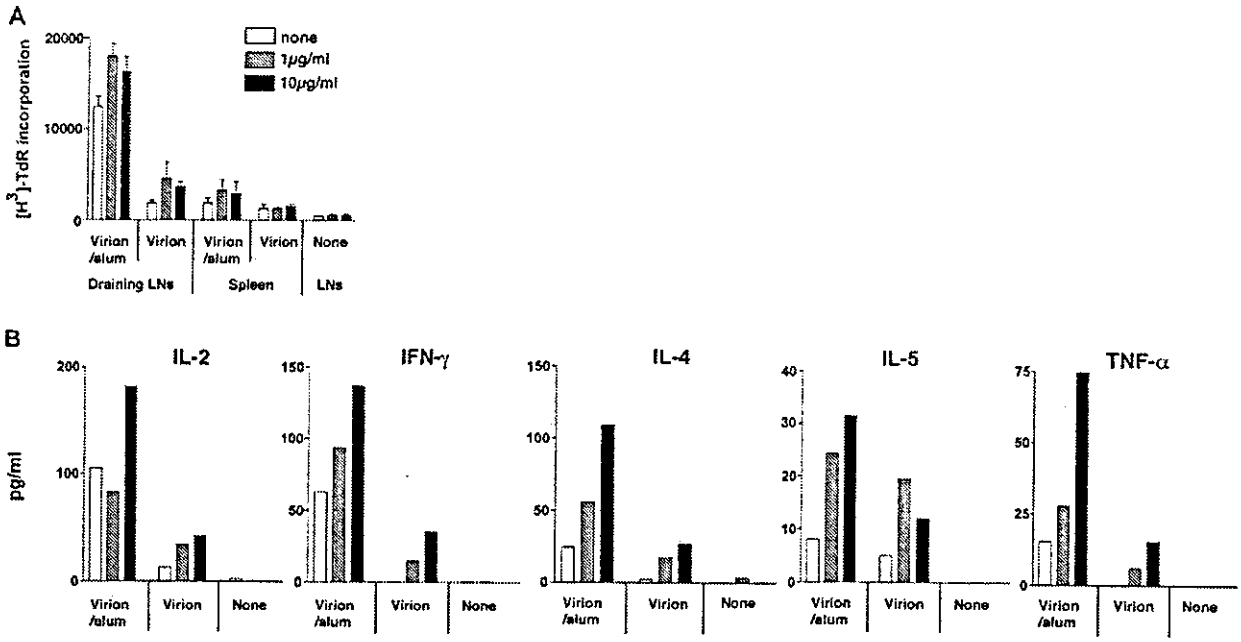

Fig. 5. *In vitro* responses of SARS-CoV-specific T cells taken from mice vaccinated with inactivated SARS-CoV. Mice were subcutaneously primed with 10 μg of UV-inactivated SARS-CoV virion, or virion with 2 mg of alum, or none, and then boosted with the same dose in their footpads at 7 weeks after priming. Draining lymph nodes and spleens were isolated at 1 week after boost and stimulated with T-cell depleted splenocytes that had been pulsed with the indicated concentration of UV-inactivated SARS-CoV virion. These cells were cultured for 2–4 days and [^{3}H]thymidine was added 8 h prior to the harvest. The peak response on day 4 after cultivation is shown in (A). (B) Culture supernatant was collected at day 2–4 post cultivation and the level of IL-2, IFN-γ, IL-4, IL-5 and TNF-α was determined by CBA kit. The maximum cytokine production at day 4 is shown. Results are representative of two separate experiments.

structures such as hepatitis B virus surface antigen-based, HIV-1 Gag-based and Ty virus-like particles have been shown to elicit humoral as well as cellular immune responses (19), these particulates probably have comparable dimensions and structures to the pathogens that are targeted for uptake by APCs to facilitate the induction of potent immune responses. The antibodies elicited in mice vaccinated by the current protocol with or without adjuvant recognized both the S and N proteins of SARS-CoV and were able to neutralize the infection of virus to Vero E6 cells. However, serum anti-SARS-CoV IgA antibody was not detectable, probably owing to the route of vaccination. In addition, the present vaccination protocol caused T cell response at the regional lymph nodes, although it did not allow for the induction of a sufficient cellular immune response systemically.

We show here the potentiality of subcutaneous injection of inactivated virion with alum, which is utilized for most of current human vaccinations. Alum has been used as an adjuvant for vaccines such as diphtheria, pertussis and tetanus, and these vaccines have a long safety record for human use (20). We observed that the addition of alum to the vaccine formula resulted in a large augmentation of serum IgG_1 production, but not IgG_{2a} production. The level of IgG_1 in alum-vaccinated mice reached a level similar to that found in hyper-immunized mice, which were subcutaneously injected with 5 μg of inactivated virion emulsified with a complete Freund adjuvant, followed by consecutive three-times intravenous boosters with 2 μg of virion. Alum is known to selectively stimulate an IgG_1 dominant, type 2 immune response [reviewed in (21)]. Activation of complement by alum could contribute to the type 2-biased immune response partly via an inhibition of IL-12 production. Interestingly, a quite recent report demonstrated that an alum-induced $Gr1^+$ myeloid cell population produced IL-4 and activated B-cells (22).

There are various diseases associated with animal coronavirus infection. The clinical manifestations of the disease and the correlates of protection with immunity have been studied extensively in these animal coronavirus infections [reviewed in (7)]. Although antibodies and T cells may play a role in exacerbating the pathology in some animal coronavirus infections (23,24), both humoral and cellular immune responses are known to contribute to protection against coronavirus infection. In murine hepatitis virus, a Group 2 coronavirus, the mortality of susceptible mice was partially prevented by the transfer of immune serum containing neutralizing antibody prior to challenge (25). Recently, Zhi-yong *et al.* reported in the murine acute infection model that the neutralizing antibody elicited by vaccination of DNA encoding S was protective, but cellular components of vaccinated mice were not required for the inhibition of viral replication (26). Because a twice parenteral administration of inactivated virion with alum induced a high level of antibodies that are able to neutralize SARS-CoV, this vaccination protocol may have a certain effect on the protection of humans from SARS-CoV infection.

We observed that two successive inoculations with inactivated virus at 7 week intervals generated SARS-CoV-specific

T cells. These cells were restimulated with the irradiated virus *in vitro*, but their response was low in terms of the level of proliferation and production of INF-γ and IL-2. However, irrespective of vaccination protocols with or without alum adjuvant, virus-primed T cells of vaccinated animals were capable of producing IL-4 at high levels upon *in vitro* stimulation, comparable to other reports for a variety of vaccination studies (27,28). This outlook seems compatible with the idea that the present vaccine protocol may tend to select T-cell subsets with Th2 phenotype. However, it remains to be elucidated whether such T cells may exhibit serological memory phenotype and persist in the immune system after vaccination as long as memory B cells, which may persist more than 180 days post vaccination. In addition, further analysis is needed to clarify whether T cell response is a crucial factor for long-term protection against SARS-CoV infections.

Efforts to develop a SARS-CoV vaccine have been carried out by many profitable or non-profitable organizations in various ways. For example, it has recently been reported that the combination of adenovirus vector expressing SARS-S, -M or -N protein elicited a neutralizing capacity in serum and N-specific T-cell response in rhesus macaques (29). However, it is still uncertain whether or not the immunity against only these components of SARS-CoV is sufficient for virus protection. SARS-CoV tends to cause replication errors, which may allow the virus to escape the host-immune response and result in a seasonal outbreak. From this point of view, it resembles influenza virus. In influenza virus, inactivated HA vaccine showed incomplete protection but had a certain efficacy and safety record for a long period of time. Indeed, this approach has been used in the veterinary field, such as with the bovine coronavirus (30) and canine coronavirus (31). These advantages make a whole killed virion a prime candidate for a SARS vaccine, even if it may not have the best protective ability.

Unfortunately, no information is available so far on the immune correlates of protection against human coronaviruses, including SARS-CoV. In consideration that SARS-CoV transmission occurs by direct contact with droplets or by the fecal oral route, mucosal secretary IgA in both the lower respiratory tract and digestive tract seem to be crucially important. Failure to induce IgA-type antibodies in a current systemic vaccination method should be improved. Notably, IgA antibodies were detectable in the sera and bronchoalveolar lavage fluid obtained from mice hyper-immunized with UV-irradiated virus (data not shown). Therefore, if a non-toxic and more potent adjuvant becomes available for human use, the subcutaneous injection of inactivated virion would become an effective vaccination method to reduce the number of susceptible people.

In the future, it will be necessary to determine whether or not the inactivated whole virion vaccine possesses protective ability against SARS-CoV infection by the use of adequate animal models. Furthermore, whether the alum addition augmented the protection and the effective period of SARS-CoV virion vaccination should be addressed, because currently used inactivated influenza virus whole virion vaccine is significantly effective without any adjuvant. Meanwhile, we also need to develop a potent adjuvant for induction of a much stronger mucosal immunity, in addition to evaluating available methods of virion inactivation.

Acknowledgements

We thank Ms R. Ishida, Ms Y. Kaburagi and Mr Y. Kimishima for their excellent technical help. This work was supported by a grant from the Ministry of Public Health and Labor of Japan.

Abbreviations

ACE2	angiotensin-converting enzyme 2
ASC	antibody-secreting cell
E	envelope
M	membrane
N	nucleocapsid protein
SARS	severe acute respiratory syndrome
SARS-CoV	SARS-associated coronavirus
S	spike protein

References

1 Drosten, C., Gunther, S., Preiser, W. *et al.* 2003. Identification of a novel coronavirus in patients with severe acute respiratory syndrome. *N. Engl. J. Med.* 348:1967.
2 Ksiazek, T. G., Erdman, D., Goldsmith, C. S. *et al.* 2003. A novel coronavirus associated with severe acute respiratory syndrome. *N. Engl. J. Med.* 348:1953.
3 Marra, M. A., Jones, S. J., Astell, C. R. *et al.* 2003. The genome sequence of the SARS-associated coronavirus. *Science* 300:1399.
4 Rota, P. A., Oberste, M. S., Monroe, S. S. *et al.* 2003. Characterization of a novel coronavirus associated with severe acute respiratory syndrome. *Science* 300:1394.
5 Holmes, K. V. and Enjuanes, L. 2003. Virology. The SARS coronavirus: a postgenomic era. *Science* 300:1377.
6 Liu, X., Shi, Y., Li, P., Li, L., Yi, Y., Ma, Q. and Cao, C. 2004. Profile of antibodies to the nucleocapsid protein of the severe acute respiratory syndrome (SARS)-associated coronavirus in probable SARS patients. *Clin. Diagn. Lab. Immunol.* 11:227.
7 De Groot, A. S. 2003. How the SARS vaccine effort can learn from HIV—speeding towards the future, learning from the past. *Vaccine* 21:4095.
8 Li, W., Moore, M. J., Vasilieva, N. *et al.* 2003. Angiotensin-converting enzyme 2 is a functional receptor for the SARS coronavirus. *Nature* 426:450.
9 Collins, R. A., Knobler, R. L., Powell, H. and Buchmeier, M. J. 1982. Monoclonal antibodies to murine hepatitis virus-4 (strain JHM) define the viral glycoprotein responsible for attachment and cell–cell fusion. *Virology* 119:358.
10 Fleming, J. O., Stohlman, S. A., Harmon, R. C., Lai, M. M., Frelinger, J. A. and Weiner, L. P.1983. Antigenic relationship of murine coronaviruses: analysis using monoclonal antibodies to JHM (MHV-4) virus. *Virology* 131:296.
11 Jackwood, M. W. and Hilt, D. A. 1995. Production and immunogenicity of multiple antigenic peptide (MAP) constructs derived from the S1 glycoprotein of infectious bronchitis virus (IBV). *Adv. Exp. Med. Biol.* 380:213.
12 Anton, I. M., Gonzalez, S., Bullido, M. J., Corsin, M., Risco, C., Langeveld, J. P. and Enjuanes, L. 1996. Cooperation between transmissible gastroenteritis coronavirus (TGEV) structural proteins in the *in vitro* induction of virus-specific antibodies. *Virus Res.* 46:111.
13 Ishii, K., Ueda, Y., Matsuo, K. *et al.* 2002. Structural analysis of vaccinia virus DIs strain: application as a new replication-deficient viral vector. *Virology* 302:433.
14 Storch, G. A. 2001. Diagnostic virology. In Knipe, D. M., Howley, P. M., ed., *Fields Virology*, 4th edn. Lippincott Williams & Wilkins, Philadelphia, PA. pp. 493–531.
15 Benner, R., Hijmans, W. and Haaijman, J. J. 1981. The bone marrow: the major source of serum immunoglobulins, but still a neglected site of antibody formation. *Clin. Exp. Immunol.* 46:1.
16 Slifka, M. K., Matloubian, M. and Ahmed, R. 1995. Bone marrow is a major site of long-term antibody production after acute viral infection. *J. Virol.* 69:1895.
17 Schmidt, O. W. and Kenny, G. E. 1982. Polypeptides and functions of antigens from human coronaviruses 229E and OC43. *Infect. Immun.* 35:515.

18 Xiao, X., Chakraborti, S., Dimitrov, A. S., Gramatikoff, K. and Dimitrov, D. S. 2003. The SARS-CoV S glycoprotein: expression and functional characterization. *Biochem. Biophys. Res. Commun.* 312:1159.
19 Singh, M. and O'Hagan, D. 1999. Advances in vaccine adjuvants. *Nat. Biotechnol.* 17:1075.
20 Clements, C. J. and Griffiths, E. 2002. The global impact of vaccines containing aluminium adjuvants. *Vaccine* 20 (Suppl. 3): S24.
21 HogenEsch, H. 2002. Mechanisms of stimulation of the immune response by aluminum adjuvants. *Vaccine* 20 (Suppl. 3): S34.
22 Jordan, M. B., Mills, D. M., Kappler, J., Marrack, P. and Cambier, J. C. 2004. Promotion of B cell immune responses via an alum-induced myeloid cell population. *Science* 304:1808.
23 Weiss, R. C. and Scott, F. W. 1981. Antibody-mediated enhancement of disease in feline infectious peritonitis: comparisons with dengue hemorrhagic fever. *Comp. Immunol. Microbiol. Infect. Dis.* 4:175.
24 Wu, G. F., Dandekar, A. A., Pewe, L. and Perlman, S. 2001. The role of CD4 and CD8 T cells in MHV-JHM-induced demyelination. *Adv. Exp. Med. Biol.* 494:341.
25 Pope, M., Chung, S. W., Mosmann, T., Leibowitz, J. L., Gorczynski, R. M. and Levy, G. A. 1996. Resistance of naive mice to murine hepatitis virus strain 3 requires development of a Th1, but not a Th2, response, whereas pre-existing antibody partially protects against primary infection. *J. Immunol.* 156:3342.
26 Yang, Z. Y., Kong, W. P., Huang, Y., Roberts, A., Murphy, B. R., Subbarao, K. and Nabel, G. J. 2004. A DNA vaccine induces SARS coronavirus neutralization and protective immunity in mice. *Nature* 428:561.
27 Mazumdar, T., Anam, K. and Ali N. 2004. A mixed Th1/Th2 response elicited by a liposomal formation of *Leishmania* vaccine instructs Th1 responses and resistance to *Leishmania donovani* in susceptible BALB/c mice. *Vaccine* 22:1162.
28 Nicollier-Jamot, B., Ogier, A., Piroth, L., Pothier, P. and Kohli, E. 2004. Recombinant virus-like particles of a norovirus (genogroup II strain) administered intranasally and orally with mucosal adjuvants LT and LT(R192G) in BALB/c mice induce specific humoral and cellular Th1/Th2-like immune responses. *Vaccine* 22:1079.
29 Gao, W., Tamin, A., Soloff, A., D'Aiuto, L., Nwanegbo, E., Robbins, P. D., Bellini, W. J., Barratt-Boyes, S. and Gambotto, A. 2003. Effects of a SARS-associated coronavirus vaccine in monkeys. *Lancet* 362:1895.
30 Takamura, K., Matsumoto, Y. and Shimizu, Y. 2002. Field study of bovine coronavirus vaccine enriched with hemagglutinating antigen for winter dysentery in dairy cows. *Can. J. Vet. Res.* 66:278.
31 Pratelli, A., Tinelli, A., Decaro, N., Cirone, F., Elia, G., Roperto, S., Tempesta, M. and Buonavoglia, C. 2003. Efficacy of an inactivated canine coronavirus vaccine in pups. *New Microbiol.* 26:151.